ELSEVIER

Contents lists available at ScienceDirect

International Journal of Heat and Mass Transfer

journal homepage: www.elsevier.com/locate/hmt



Virtual and physical experiments of encapsulated phase change material embedded in building envelopes



Chunlin Wu, Zhenhua Wei, Huiming Yin*

Department of Civil Engineering and Engineering Mechanics, Columbia University, 610 Seeley W. Mudd 500 West 120th Street, New York, 10027, United States

ARTICLE INFO

Article history: Received 2 December 2020 Revised 19 January 2021 Accepted 6 February 2021 Available online 9 March 2021

Keywords: Temperature gradient Boundary element method Equivalent inclusion method Phase change material Heat capacity method

ABSTRACT

This paper investigates the temperature and heat flux fields of composite materials containing phase change materials (PCM) for energy efficient buildings. A novel numerical method validated by accurately controlled laboratory experiments is presented for virtual experiments of more complex applications. Considering a finite bounded domain containing one inclusion, the Green's function technique has been applied to obtain the transient heat transfer response caused by sources on inclusion domains and prescribed boundaries. Based on the Eshelby's equivalent inclusion method (EIM), the thermal property mismatch between the PCM particle and matrix phases is simulated with a uniformly distributed eigen-temperature gradient field and a fictitious heat source on the particle. Through the combination of EIM and boundary element method, namely the iBEM, the temperature field can be written in terms of the temperature and heat flux on the boundary and the distributed eigen-temperature gradient and heat source on the particle. By using the equivalent heat flux conditions and the specific heat-temperature relationship, the eigen-temperature gradient and fictitious heat source can be solved and the temperature field of the bounded domain can be calculated. This new numerical method has been verified by the finite element simulation and validated with the laboratory measurements of the transient heat transfer within a building block containing a PCM capsule. Parametric studies have also been conducted to study the influences of the PCM location and volume fraction on the temperature field of composites with multiple particles. The virtual experiments demonstrate the energy saving and phase delay by using the PCM-concrete wall panel. This method will be very useful for the design and thermal analysis of building envelopes.

© 2021 Elsevier Ltd. All rights reserved.

1. Introduction

About 20% of total energy consumption in the U.S. comes from the heating and cooling of buildings using conventional sources like fossil fuels and electricity [1]. The applications of phase change materials (PCMs) in building envelopes have proven to be an effective method to mitigate heating/cooling loss and control the temperature variations across building walls [2–5], because PCMs can absorb heat during a hot period and release stored heat during a cold period [6,7], thereby significantly reducing the temperature variation inside the building. The use of PCMs has also been shown as a means to shift the energy consumption peak and stabi-

 $\it E-mail\ addresses:\ cw3056@columbia.edu\ (C.\ Wu),\ itzwei@spdlabs.com\ (Z.\ Wei),\ yin@civil.columbia.edu\ (H.\ Yin).$

lize power grid, which provides more resilient energy services and infrastructure [8,9].

PCM embedded building materials may consist of different types and amounts of cement compositions and PCMs reflected in a wide range of thermalphysical properties [10,11]. In the design of energy-efficient building materials, it is critical to select appropriate PCM for a certain mix formula to achieve the desired thermal performance before mixing them together. While numerous studies qualitatively investigated the influences of PCMs on the thermal response of cementitious building materials in terms of flattening temperature curves and delaying peak temperature, it is highly demanded of the quantitative understanding and accurate prediction of the overall performance to develop performance-based design criteria of the cementitious composites.

To simulate the heat transfer and phase change of a PCM particulate composite, there are three schools of models based on the grid-fixed grid [12–14], deforming grid [15] and hybrid grid

^{*} Corresponding author.

Nomenclature

Superscripts

* Eigen field, used in equivalent inclusion method

Quantities of the Ith inhomogeneity

Physical quantities

 α Thermal diffusivity (m^2/s)

 ΔH_m Latent heat of fusion per unit mass of PCM

 Δt Time interest between points in the time coordi-

nate

 Δu Range of phase change temperature window

 ϵ Temperature gradient Λ Inhomogeneity domain $\Phi_{\it p}$ Volume fraction of PCM

 C_p Specific heat on unit volume $(J/m^3 \circ C)$

 h_i, h_o Heat transfer coefficient of indoor / outdoor con-

crete surfaces

 $J_{f,i}$ The Eshelby's tensor for heat source k Thermal conductivity (W / m $^{\circ}$ C)

 M_f The Eshelby's tensor for eigen-temeprature gradient

Q Heat source (W/m^3) q Heat flux (W/m^2)

 t_{Ω} Duration of the time domain (hour)

u Temperature (°C)

 u_c Midpoint of the phase change temperature window

Subscripts

0, F Initial / ending state of the quantities
 bc Prescribed boundary conditions
 f The fth point in the time coordinate

[16] models. The fixed grid models employ the auxiliary equations to track the solid/liquid boundary and have wide applications. Based on the name of thermal quantities in the auxiliary equations for the latent heat evolution of the PCM, the enthalpy, heat capacity, and heat source methods are introduced in the literature. The enthalpy method combines the specific heat and latent heat fusion as an auxiliary temperature-enthalpy function [15,17-19]. The heat capacity method, proposed by Hsiao [20], approximates the apparent heat capacity as a function of temperature [13,21]; whereas the heat source method divides the enthalpy term into the enthalpy method with specific heat and latent heat, where the latent heat serves as a heat source [22,23]. Different from the above fixed grid models, the deforming grid model explicitly tracks the solid/liquid boundary since the grid nodes can move along with the boundary layer; whereas the hybrid grid model combines the merits of the above two models, and uses the fixed gird and front tracking scheme together [10].

Robust design of PCM embedded building materials requires quantitative evaluation of the influence of PCMs on their thermal performance. Many models and methods were developed to characterize the heat flux within building materials with inhomogeneities and phase transition of PCMs in the literature. Typically, for a bounded domain with prescribed boundary conditions and initial conditions, the heat equation can be solved by finite difference method (FDM) [17], finite element method (FEM) [24,25] and boundary element method (BEM) [26,27]. FDM discretizes the time and spatial domain instead of taking derivatives, and it is usually applied to solve diffusion equations. However, the solutions of FDM are sensitive to time discretization and discontinuity issues [28]. FEM requires discretization of the entire spatial domain including the inhomogeneities, and its accuracy is dependent on the quality of mesh, which is a tremendous challenge when micro-sized PCMs are incorporated in building envelopes. In contrast, BEM only

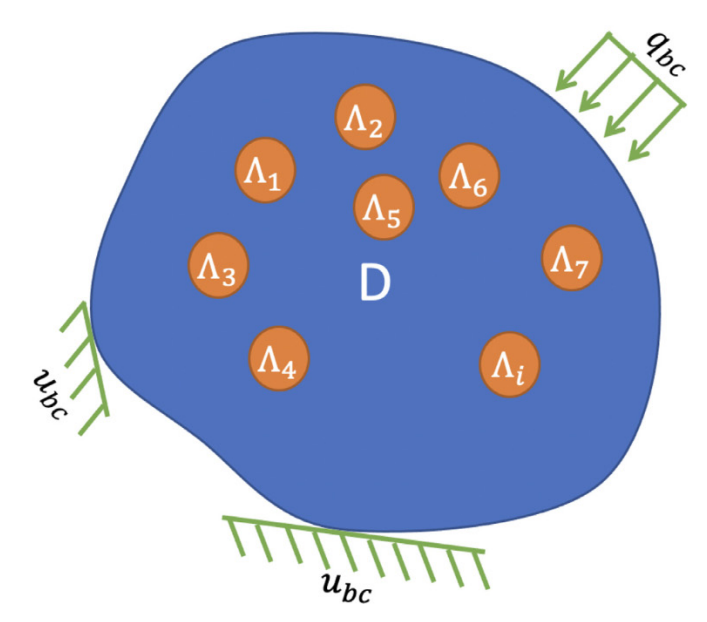


Fig. 1. Schematic illustration of multiple inhomogeneities embedded in a domain $\mathcal D$ with prescribed boundary conditions.

meshes the boundary of the domain but requires fundamental solution for each material domain. For a composite containing many PCM particles, it is still very expensive to mesh each particle surface and simulate an actual composite with interface continuity conditions.

Our recent work has revealed that the inhomogeneity problem of PCM particles in a matrix can be transferred to an inclusion problem based on Eshelbys equivalent inclusion method [29–31] that bridges the macro-behavior of a composite to its microstructural composition. Nevertheless, for a domain with prescribed geometry and boundary conditions, only adopting EIM or micromechanical models cannot solve the thermal fields as it requires the specific Green's function with boundary conditions. In addition, it is inconvenient to derive Green's function for all types of the domain, especially for some irregular geometry [32–34]. Therefore, an inclusion-based boundary element method (iBEM) provides advantages that avoid meshing the particle surface and can use the fundamental solution or Green's function for the infinite domain.

In this study, the authors coupled EIM, BEM and the heat capacity method to solve the heat transfer problem where phase change occurs in a composite containing spherical PCM capsules under sinusoidal air temperature variations. By assembling the equivalent flux equations of the particle into BEM global matrix, the PCM particle-boundary interaction as well as particle-particle interactions are simulated during the phase change process and the size effects of the samples are demonstrated simultaneously. After the thermal fields of the bounded domain are validated by the experimental results and verified by the finite element simulation, this method has been used in the virtual experiments of PCM composites for building applications. This numerical method provides a simple yet rigorous tool to design and evaluate the thermal benefits of phase-change building materials.

2. Boundary element method

Consider a spatial domain D subjected to boundary conditions such as a heat flux of q_{bc} and a prescribed temperature of u_{bc} during time domain Ω with a given initial condition (Fig. 1). Using the Green's function technique, the temperature field at ${\bf x}$ and t can be expressed by boundary integral over the time domain as

[27,32,35]

$$u(\mathbf{x},t) = \int_{D} G(\mathbf{r},t)u^{0}d\mathbf{x}' + \frac{1}{C_{p}} \int_{\Lambda} \int_{\Omega} G(\mathbf{r},\tau)Q(\mathbf{x}',t')dt'd\mathbf{x}' + \alpha \int_{\partial D} \int_{\Omega} G(\mathbf{r},\tau)q_{bc}dt'd\mathbf{x}' - \alpha \int_{\partial D} \int_{\Omega} T(\mathbf{r},\tau)u_{bc}dt'd\mathbf{x}'$$
(1)

where the transient Green's function in the infinite domain and its derivative are written as

$$G(\mathbf{r},\tau) = \frac{1}{(4\pi\alpha\tau)^{\frac{3}{2}}} e^{\frac{-r^2}{4\alpha\tau}} H(\tau)$$

$$T(\mathbf{r},\tau) = -\frac{2\pi r_i n_i}{(4\pi\alpha\tau)^{\frac{5}{2}}} e^{\frac{-r^2}{4\alpha\tau}} H(\tau)$$
(2)

in which $\mathbf{r} = \mathbf{x} - \mathbf{x}'$, $\tau = t - t'$ and $\alpha = \frac{k}{C_p}$, as C_p and k denote the specific heat on unit volume and thermal conductivity, respectively. The superscript 0 represents the initial condition, and Q and Λ are the heat source and its domain; $H(\tau)$ is the Heaviside function; the Green's function $G(\mathbf{r}, \tau)$ is also called the fundamental solution due to an impulse heat source at \mathbf{x}' and time t'; $T(\mathbf{r}, \tau)$ is the derivative of the Green's function with respect to the surface normal n [27]; the first term in Eq. (1) involves the initial temperature field. To numerically evaluate the boundary integral in Eq. (1), Gupta [27] interchanged the integral sequence and derived the analytical form with respect to time Ω from t_0 to t_F , in which t_0 and t_F are the start time and ending time (or the observing time). Discretize Ω by N_F time steps with time coordinate $t_i, i = 0, 1, 2, \dots, N_F$ and the time intervals $t_i - t_{i-1}$ $(i = 1, 2, \dots, N_F)$ are not necessarily to be the same, although in this paper, equal time intervals are used for convenience. Assume that the thermal responses remain the same over one time step, thus the influences from thermal source during the time interval t_{f-1} to t_f and location \mathbf{x}' are handled by time integral of the Green's function over the time interval of $t_f - t_{f-1}$. The time integrals of G and T defined in Eq. (2) for each time step are written as $\overline{G}(\mathbf{r}, t_{\Omega}, \Delta t)$ and $\overline{T}(\mathbf{r}, t_{\Omega}, \Delta t)$, where t_{Ω} is the duration of the overall time domain, i.e. $t_{\Omega} = t_F - t_f$, and the time interval is defined as $\Delta t = t_f - t_{f-1}$. They can be explicitly expressed with the incomplete gamma functions (IGF), which are presented in Appendix A. Eq. (A.2) can be numerically integrated by the approximation of temperature and heat flux fields of each element with the temperature and heat flux field provided by the corresponding shape function as,

$$u(\mathbf{x},t) = \int_{D} G(\mathbf{r},t) u^{0} d\mathbf{x}' + \frac{1}{C_{p}} \int_{\Lambda} \int_{\Omega} G(\mathbf{r},\tau) Q(\mathbf{x}',t') dt d\mathbf{x}'$$
$$+ \sum_{f=1}^{N_{F}} \sum_{l=1}^{N_{e}} \sum_{i=1}^{N_{n}} (U_{i} q_{i}^{bc})_{f} - \sum_{f=1}^{N_{F}} \sum_{l=1}^{N_{e}} \sum_{i=1}^{N_{n}} (H_{i} u_{i}^{bc})_{f}$$
(3)

where N_e and N_n are the numbers of elements and nodes, respectively, in the corresponding element; U_i and H_i are the boundary integrals with the specific shape functions, i.e. $(U_i)_f = \alpha \int_{\partial D} \overline{G}(\mathbf{r}, t_{\Omega}, \Delta t) N_i ds$ and $(H_i)_f = \alpha \int_{\partial D} \overline{T}(\mathbf{r}, t_{\Omega}, \Delta t) N_i ds$, in which N_i denotes the shape function; the subscript f the thermal source active time interval during time t_{f-1} and t_f . Based on the concept of Green's function, the heat fields at any future time are dependent on the past heat quantities, it is necessary to store the previous matrices and boundary solutions.

3. Inclusion problem for infinite and finite domain

Without the loss of generality, consider an infinite homogeneous domain, D_{inf} , containing an eigen-temperature gradient ϵ_i^* and heat source Q^* at the subdomain Λ_I . Here eigen-temperature gradient denotes a prescribed temperature gradient that does not

contribute to any heat flux, i.e. $q_i = -k(u_{,i} - \epsilon_i^*)$ [36,37]. Now introduce a fictitious quantity $Q' = Q^* - k\epsilon_{i,i}^*$, which is an equivalent heat source caused by ϵ_i^* and Q^* . The temperature field caused by the source Q' in Eq. (1) can be rewritten as [32,33],

$$u(\mathbf{x},t) = \frac{\alpha}{k} \sum_{f=1}^{N_F} \{ \int_{\Lambda_I} \overline{G}(\mathbf{r}, t_{\Omega}, \Delta t) d\mathbf{x}'(Q^*)_f$$

$$- \int_{\partial \Lambda_I} \overline{G}(\mathbf{r}, t_{\Omega}, \Delta t) k n_i' dS(\epsilon_i^*)_f$$

$$- \frac{\partial}{\partial x_i} \int_{\Lambda_I} \overline{G}(\mathbf{r}, t_{\Omega}, \Delta t) k d\mathbf{x}'(\epsilon_i^*)_f \}$$

$$(4)$$

where the subscript f represents the thermal quantities existing during time t_{f-1} and t_f . Here only the second term in Eq. (1) exists and the Gauss theorem is used to transfer the domain integral to the boundary of the subdomain Λ_I . In Eq. (4), the fictitious quantity only exists in the subdomain Λ_I , and the contour integral at the outer surface yields zero. Therefore, only the domain integral terms of the first and third terms in Eq. (4) exist. Introduce the domain integral terms as:

$$M_{f} = \frac{\alpha}{k} \int_{\Lambda_{I}} \overline{G}(\mathbf{r}, t_{\Omega}, \Delta t) d\mathbf{x}'$$

$$J_{f,i} = -\alpha \frac{\partial}{\partial x_{i}} \int_{\Lambda_{i}} \overline{G}(\mathbf{r}, t_{\Omega}, \Delta t) d\mathbf{x}'$$
(5)

where M_f and $J_{f,i}$ denote the influence of the eigen-temperature gradient and heat source of the inclusion (Λ_I) existing during time t_{f-1} and t_f in an infinite domain. Combined the ordinary BEM Eq. (3) and the disturbed field by fictitious quantity Eq. (4), the temperature field at \mathbf{x} ($x \in D$) can be presented as,

$$u(\mathbf{x},t) = \sum_{f=1}^{N_F} \left(\sum_{l=1}^{N_c} \sum_{i=1}^{N_n} \left[\left(U_i q_i^{bc} \right) - \left(H_i u_i^{bc} \right) \right]_f + \sum_{l=1}^{N_S} \left(M_f Q^{l*} + J_{f,i} \epsilon_i^{l*} \right) \right) + \int_D G(\mathbf{r},t) u^0 d\mathbf{x}'$$
(6)

where N_S denotes the number of subdomains. The above equation is based on the homogeneous material with the boundary effects as well as heat sources on a number of subdomains or inclusions. However, actual composites contain phase change material (PCM) particles that are different from the matrix. The same Green's function cannot be used for both PCM particles and the matrix due to the different governing equations. Traditional BEM uses boundary integrals over each material domain with the boundary continuities, which requires numerical boundary integrals on the subdomains with high computational costs. In the following, iBEM is introduced to use Eq. (6) to avoid the numerical boundary integral of the subdomains.

4. Phase change process

Following Eshelby's work [36], PCM capsules can be treated as inclusions with eigen-temperature gradient and heat source, which can be determined by the equivalence of heat flux to simulate the material mismatch. One challenge involved in the modeling is that PCMs specific heat increases during phase change. Hsiao [20] proposed a piece-wise specific heat function in terms of temperature for numerical simulation of phase change process. For a pure material, it has sharp freezing/melting temperature, thus a small temperature interval is desirable and vice versa. In general, the PCM capsules used in the building envelopes feature a comparatively larger temperature interval, measured by differential scan-

ning calorimetry (DSC) [38],

$$C_{p}(u) = \begin{cases} C_{p,s} & \text{if } u < u_{s} \\ \frac{\Delta H_{m}}{u_{h} - u_{l}} + \frac{C_{p,s} + C_{p,l}}{2} & \text{if } u_{s} \leq u \leq u_{e} \\ C_{p,l} & \text{if } u_{e} < u \end{cases}$$
(7)

where $C_{p,s}$ and $C_{p,l}$ are specific heat for the solid and liquid phases of PCM, u_s and u_e are the temperatures that the phase changing starts and ends, respectively; and ΔH_m is the latent heat fusion per unit mass of PCM. Since the volume of each PCM capsule is small, one assumption was made that the entire status of the particle can be described by spatial-averaged temperature of sampling points. Therefore, the heat capacity the entire particle can be considered as uniform.

5. Inclusion-based boundary element method for transient heat conduction with phase change process

In Section 2, the equation for the bounded inclusion problem is built with eigen-temperature gradient and fictitious heat source. EIM treats each particle with a different thermal conductivity as the same material as the matrix but an eigen-temperature gradient and a fictitious heat source are introduced to simulate the effect of material difference on the heat transfer. Therefore, the boundary value problem for a finite domain with many inhomogeneities can be solved with a uniform material with the corresponding inclusions of source field of eigen-temperature gradient and heat source. The iBEM formula combines BEM and EIM using the equivalent flux condition within the inhomogeneity domain Λ_I . For each inhomogeneity, 2 more thermal quantities, namely eigentemperature gradient and fictitious heat source, are introduced to describe the material mismatch and phase change process.

5.1. Implementation of EIM

Consider a bounded domain D with N_S embedded PCM inhomogeneities Λ_I , $I=1,2,3\ldots$. Denote material properties of matrix and inhomogeneities as k_0,C_p^0 and k_I,C_p^I , respectively, where k and C_p are thermal conductivity and specific heat, respectively. Notice that here the specific heat is based on unit volume and can be transferred from mass-based specific heat by multiplying density. The equivalent conditions are built upon the heat flux field within the inhomogeneity to match the thermal conductivity difference and product of density and specific heat at each time step as,

$$-k_0(u_{,i} + \epsilon'_i - \epsilon^*_i) = -k_I(u_{,i} + \epsilon'_i) \quad \text{in} \quad \Lambda_I$$

$$C_p^0 \frac{\partial u}{\partial t} = C_p^I \frac{\partial u}{\partial t} + Q_i^* \quad \text{in} \quad \Lambda_I$$
(8)

where the temperature gradient $u_{,i}$ can be obtained by taking derivative with respect to $x_{,i}$ in Eq. (6). Since the boundary response remains the same at each time step, thus the derivatives are only taken with the coefficients of U, H, M, J and G. As for the temperature changing rate $\frac{\partial u}{\partial t}$, it can be derived similarly as temperature gradient. Eq. (8) can be simplified as,

$$\Delta k u_{,i} = k_0 \epsilon_i^*$$

$$\Delta C_p^l \frac{\partial u}{\partial t} = Q_i^*$$
(9)

Written the temperature and its changing rate in terms of the boundary integral and volume integral over particles with ϵ_i^* and Q_i^* on each particle, one can solve for ϵ_i^* and Q_i^* .

5.2. Equivalent heat flux condition with the heat capacity method

The physics of PCM is that when the temperature is in the range of phase change temperature window, the heat capacity C_D ,

i.e. the product of density and specific heat, is larger than that in other temperature ranges. By modifying the heat equation, the left-hand side heat capacity can be expressed as $C_p(u)$, which is the function of temperature. As assumed in Section 4, a spatialaveraged specific heat is considered for the entire PCM particle, which is a piece-wise function of temperature. Therefore, a heat source term Q_{rc}^{I} is used to match the heat capacity difference, which is similar to inclusion problem with fictitious heat source. Although Q_{rc}^{I} and Q_{t}^{*} are introduced for PCM particle in the mushy state with solid/liquid co-existing respectively, they both serve to match the heat capacity difference. Therefore, it is natural to consider a heat source $Q_I^*(u)$ as a general form for heat capacity mismatch in Eqs. (7) and (9). In Eq. (6), the temperature at any point and time, can be expressed. The heat source term Q_I^* is dependent on the temperature changing rate and the heat capacity difference ΔC_p^I . Employing a backward finite difference scheme [39], the temperature changing rate at time step n is written as

$$\frac{\partial u}{\partial t} = \frac{u^n - u^{n-1}}{t^n - t^{n-1}} \tag{10}$$

Since the time interval and temperature at the previous time step are known, the key of the scheme is to express the temperature at current time step by Eq. (6). According to Hsiao's work [20], the heat capacity of the PCM particle is computed at the previous time step. The explicit scheme will be presented in Eq. (14) in the next subsection.

5.3. Assembly of the global matrix of iBEM

To solve the problem, the global matrix of iBEM can be assembled as follows: Firstly, assemble the boundary element equation related with boundary nodes' temperature and surface element fluxes. Secondly, assemble EIM equations and phase change process constraint equations of Eq. (9). In Section 5.1 and Section 5.2, the equations will be solved for the material properties mismatch and phase change process simultaneously with modified coefficients of the variables ϵ^* , Q^* . The initial conditions are implemented in Eq. (6), where they are multiplied with Green's function and then integrated in the spatial domain. The implementation of boundary conditions are the same as BEM, which involves computed coefficients matrix multiplying the boundary variable vectors. The superscript (') denote the spatial derivative and let the spatial integral of Green's function be G_{int} . Following the pioneer work on BEM [27], a direct iBEM for phase change problem is shown below. Based on Eq. (8), the modified EIM equation is written as,

$$(\epsilon_{i}^{l*})_{f} = \frac{\Delta k}{k_{0}} \left\{ \sum_{c=1}^{f} \sum_{l=1}^{N_{e}} \sum_{i=1}^{N_{n}} \left[(U_{i}'q_{i}^{bc}) - (H_{i}'u_{i}^{bc}) \right]_{c} + \sum_{l=1}^{N_{S}} (M'Q^{l*} + J_{i}'\epsilon_{i}^{l})_{c} + C_{int}'(\mathbf{r}, t)u^{0} \right\}$$

$$= \frac{\Delta k}{k_{0}} \left\{ \sum_{l=1}^{N_{e}} \sum_{i=1}^{N_{n}} \left[(U_{i}'q_{i}^{bc})_{f} - (H_{i}'u_{i}^{bc})_{f} \right] + \sum_{l=1}^{N_{S}} \left[(J_{i}'\epsilon_{i}^{l*})_{f} + (M'Q^{l*})_{f} \right] \right\}$$

$$+ \frac{\Delta k}{k_{0}} \left\{ \sum_{c=1}^{f-1} \sum_{l=1}^{N_{e}} \sum_{i=1}^{N_{n}} \left[(U_{i}'q_{i}^{bc}) - (H_{i}'u_{i}^{bc}) \right]_{c} + \sum_{l=1}^{N_{S}} \left(M'Q^{l*} + J_{i}'\epsilon_{i}^{l} \right)_{c} + G_{int}'(\mathbf{r}, t)u^{0} \right\}$$

$$(11)$$

where the subscripts f and c represent the thermal quantities existing during time t_{f-1}, t_f and t_{c-1}, t_c , respectively. Combining the

coefficient of ϵ_i^{I*} yields,

$$\sum_{l=1}^{N_{e}} \sum_{i=1}^{N_{n}} \left[\left(U_{i}^{'} q_{i}^{bc} \right)_{f} - \left(H_{i}^{'} u_{i}^{bc} \right)_{f} \right] \\
+ \sum_{l=1}^{N_{S}} \left[\left(\left(J_{i}^{'} - \frac{k_{0}}{\triangle k} \right) \epsilon_{i}^{l*} \right)_{f} + \left(M^{'} Q^{l*} \right)_{f} \right] \\
+ \sum_{c=1}^{f-1} \sum_{l=1}^{N_{e}} \sum_{i=1}^{N_{n}} \left[\left(U_{i}^{'} q_{i}^{bc} \right) - \left(H_{i}^{'} u_{i}^{bc} \right) \right]_{c} \\
+ \sum_{l=1}^{N_{S}} \left(M^{'} Q^{l*} + J_{i}^{'} \epsilon_{i}^{l} \right)_{c} + G_{int}^{'} (\mathbf{r}, t) u^{0} = 0 \tag{12}$$

where the modified coefficient of $(\epsilon_i^{I*})_f$ is $\frac{\Delta k^l}{k_0}J'_{f,i}-1$ and $\Delta k^l=k_0-k_I$. Note that the modified coefficient does not exist in the domain of dependence except the current time step matrix. Similarly, the modified coefficient for the heat source can be obtained as $M_f-\frac{t_f-t_{f-1}}{\Delta C_p^{I-1}}$ and $\Delta C_p^I=C_p^0-C_p^I$. Finally, the modified constraint equation of PCM particle temperature can be expressed. Note that the heat capacity C_p^I is function of u_I^n , which is the spatial-average temperature of the Ith subdomain at previous time step. The constraint equation at Ith subdomain is expressed by Eq. (13),

$$\sum_{l=1}^{N_{c}} \sum_{i=1}^{N_{n}} \left[\left(U_{i} q_{i}^{bc} \right)_{f} - \left(H_{i} u_{i}^{bc} \right)_{f} \right] \\
+ \sum_{l=1}^{N_{S}} \left[\left(J_{i} \epsilon_{i}^{l*} \right)_{f} + \left[\left(M - \frac{t_{f} - t_{f-1}}{\Delta \left(C_{p} \right)^{l}} \right) Q^{l*} \right]_{f} \right] \\
+ \sum_{c=1}^{f-1} \sum_{l=1}^{N_{c}} \sum_{i=1}^{N_{n}} \left[\left(U_{i} q_{i}^{bc} \right) - \left(H_{i} u_{i}^{bc} \right) \right]_{c} + \sum_{l=1}^{N_{S}} \left(M Q^{l*} + J_{i} \epsilon_{i}^{l*} \right)_{c} + \\
+ G_{int}(\mathbf{r}, t) u^{0} - u^{l}_{f-1} = 0 \tag{13}$$

Combined the above equivalent equations with BEM equations, the main matrix and variable vectors for iBEM can be formed. To simplify the notation of main matrix, denote \overline{U} , \overline{H} , \overline{J} , \overline{M} to represent the coefficient matrix for the variable vectors $\overline{q_{bc}}$, $\overline{u_{bc}}$, $\overline{\epsilon^*}$, $\overline{Q^*}$. And denote the coefficients of initial conditions as the vector $\overline{G_0^0}$. Thus,

the direct form of the iBEM is obtained as,

$$\begin{bmatrix} C + \overline{H_f} & -\overline{J_f} & -\overline{M_f} \\ -\overline{H_f'} & \overline{J_f'} - \frac{k_0}{\Delta k} & \overline{M_f'} \\ -\overline{H_f} & \overline{J_f} & \overline{M_f} - \frac{t_f - t_{f-1}}{\Delta C_p^{-1}} \end{bmatrix} \begin{bmatrix} \overline{u_{bc}^f} \\ \overline{e_f^f} \\ \overline{Q_*^f} \end{bmatrix} - \begin{bmatrix} \overline{U_f} \\ -\overline{U_f'} \\ -\overline{U_f'} \end{bmatrix} \begin{bmatrix} \overline{q_{bc}^f} \end{bmatrix} =$$

$$- \sum_{c=1}^{f-1} \begin{bmatrix} \overline{H_c} & -\overline{J_c} & -\overline{M_c} \\ -\overline{H_c'} & \overline{J_c'} & \overline{M_c'} \\ -\overline{H_c} & \overline{J_c} & \overline{M_c} \end{bmatrix} \begin{bmatrix} \overline{u_{bc}^c} \\ \overline{e_e^c} \\ \overline{Q_*^c} \end{bmatrix} + \begin{bmatrix} \overline{U_c} \\ -\overline{U_c} \\ -\overline{U_c} \end{bmatrix} [\overline{q_{bc}^c}]$$

$$+ \begin{bmatrix} \overline{G_u^0} \\ -\overline{G_u^0} \\ -\overline{G_u^0} \end{bmatrix} [\overline{u_0}] + \begin{bmatrix} 0 \\ 0 \\ u_f^{l-1} \end{bmatrix}$$

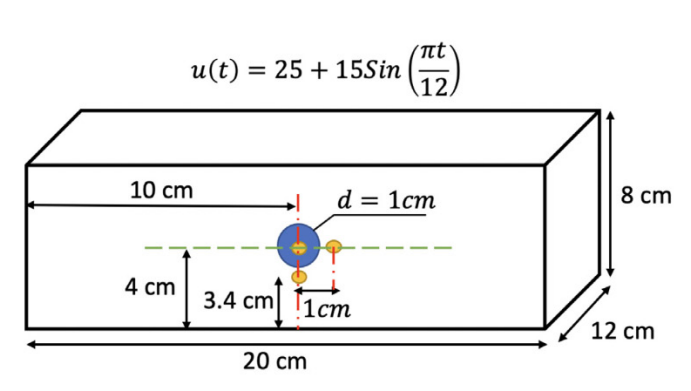
$$(14)$$

To reduce the computational cost, keeping the same time intervals, there is only one coefficient matrix to be solved and stored at each time step, which brings the influence of the beginning thermal field.

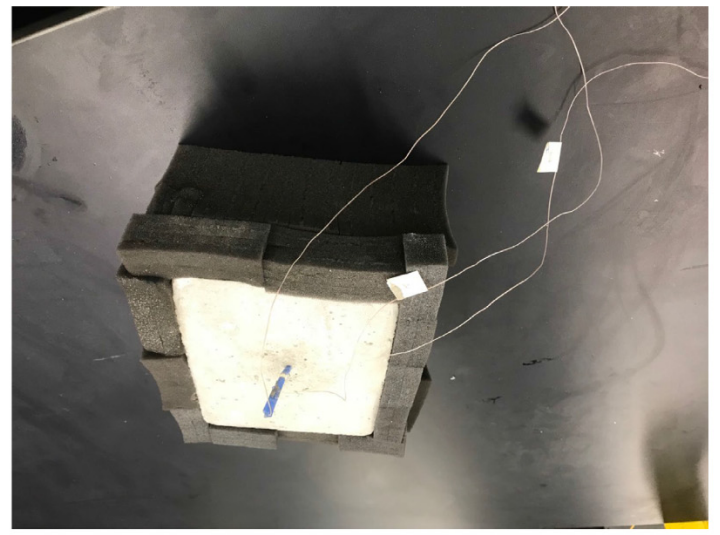
6. Numerical verification

6.1. Verification of the temperature of one centered PCM particle

The above mentioned algorithm for the phase change process has been implemented into the software package of iBEM, which combines both the EIM ([36,37]) and the BEM [33,35]. If the surface mesh elements and specific boundary conditions are known, the field can be solved. In order to verify the solver, we have prepared a concrete block with a paraffin-based PCM capsule placed at the center to resemble part of a wall panel. As shown in Fig. 2, the top surface of the block was subjected to a daily sinusoidal temperature load, $u(t) = 25 + 15Sin(\frac{\pi}{12}t)$, while other surfaces were thermally insulated. The diameter of the spherical PCM particle was 1cm and its specific heat was a function of temperature measured by the differential scanning calorimetry (DSC) shown in Fig. 3. Five Type T thermocouples with the measurement accuracy within 0.5 °C were embedded to monitor temperature evolution at different locations, as shown in Fig. 2 - inside the PCM capsule, 0.6cm below the PCM center, 1cm right to the PCM center, and top surface and air above the block. The thermal properties of



(a) Boundary conditions and geometry dimensions



(b) Experiment setup

Fig. 2. Schematic illustration of the dimensions, boundary conditions of the concrete block with a spherical PCM particle and thermal probes.

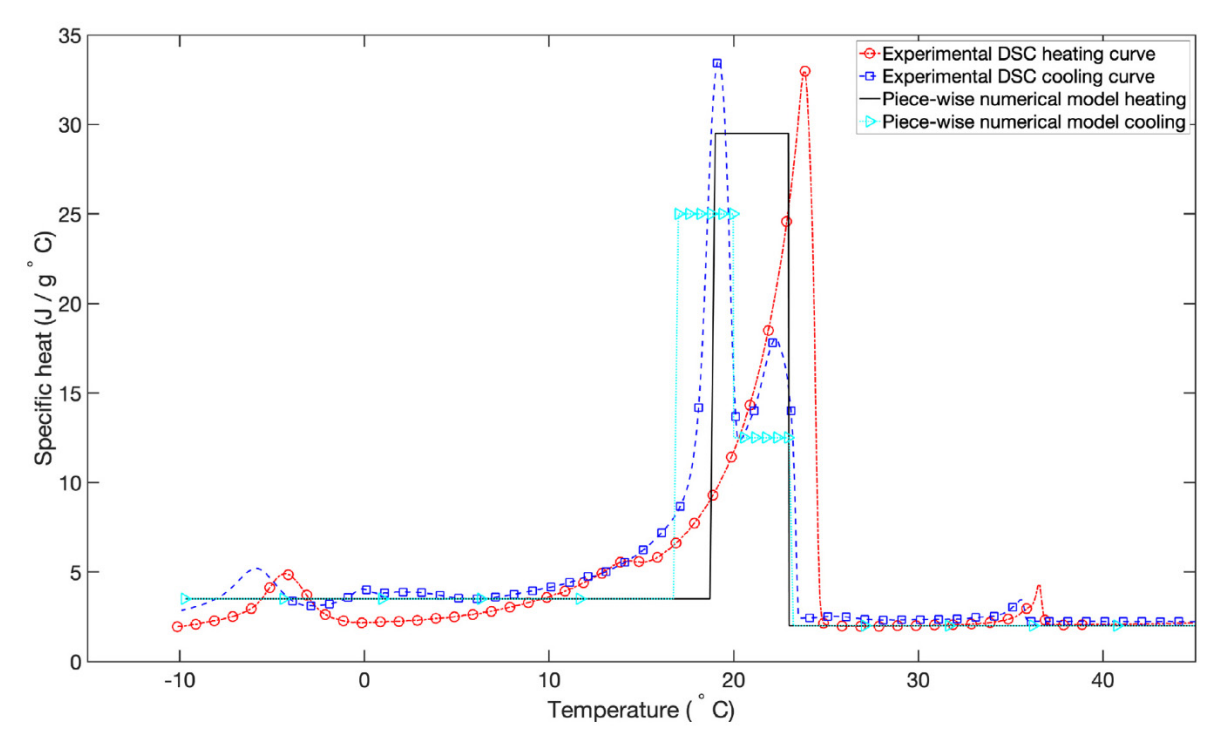


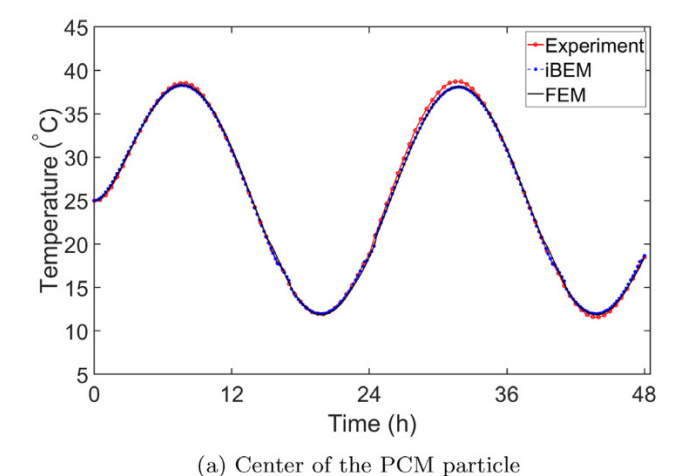
Fig. 3. Specific heat of microencapsulated PCM (MPCM24D) as a function of temperature measured by DSC with a temperature ramp rate of 1°C/min with the piece-wise numerical model of [18, 22]°C phase change temperature window (i.e for the energy prediction in Section 7.1).

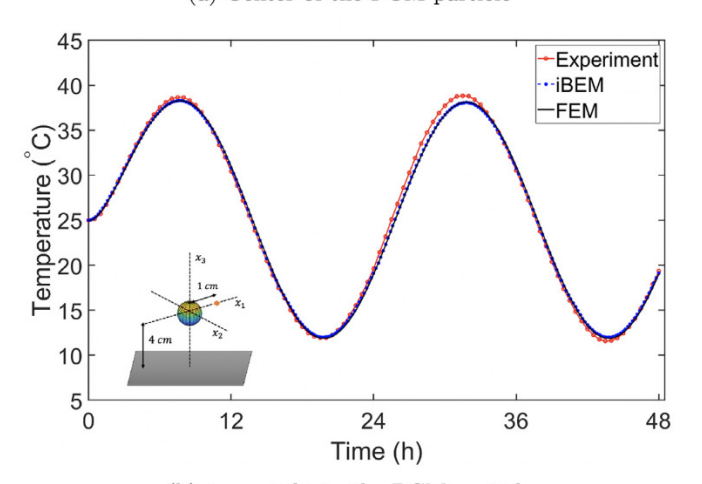
Table 1Thermal properties of the concrete and PCM.

Thermal properties of concrete and PCM			
Parameters	Values		
density of the concrete density of the PCM thermal conductivity of the concrete thermal conductivity of the PCM specific heat of the concrete latent heat of the PCM	1965 kg/m ³ 900 kg/m ³ 1 W/m°C 0.21 W/m°C 1530 J/kg°C 160 kJ/kg		

concrete and the PCM are shown in Table 1: whereas their density and thermal conductivity are considered to be constant due to the relatively small temperature change during the experiment. A commercial FEM software ANSYS was used to solve the temperature field subjected to the same boundary conditions. To prepare for the FEM simulation, the body element size was chosen as 0.5cm with a 3 times refined region for the PCM particle, which leads to the numbers of nodes and elements being 68138 and 49342, respectively. The minimum and maximum time intervals were 0.1 and 0.5 h, respectively, and the specific time intervals are automatically controlled by the software in the above range. For the phase change process to be consistent with the heat capacity method, the specific heat of the PCM was replaced by a piece-wise function with an equivalent latent heat (i.e., 160 KJ/Kg) and a 5-degree phase change window [16,21] °C. However, the specific heat - temperature relationship is different between the heating and cooling cycles. Following Kumarasamy et al. [40], the specific heat and temperature curve is constructed in Fig. 4a. During the heating process, the phase change window is [19,23] °C [38]; whereas during the cooling process, two 3-degree phase change windows are used - [17,20] and [20,23] °C - while the latent heat remains the same. In contrast, the iBEM takes advantages of surface meshing only 866 nodes and 864 quadrilateral elements. The subdomain, i.e, the PCM particle, was treated as the same material as the concrete matrix along with 3 unknowns of eigen-temperature gradient field(ϵ_i^{I*}) and 1 unknown of the fictitious source Q^{I*} at each time step. Thus, for each time step, the number of system linear equations is $N_n + 4N_S$, which is significantly less than that in the FEM modeling. The time intervals in iBEM was set to be equally 0.2 h to save the computational resources. In addition, the iBEM can use the same mesh for the particle with different sizes or locations; whereas the FEM has to re-mesh the domain.

The initial temperature of the concrete is 25 °C, and the test duration is 48h. The temperature-time curves obtained from the experiment agree well with the iBEM predictions, regardless of the location in the concrete block, as shown in Fig. 4. The FEM simulation results also show very good agreement with iBEM and experimental results, which further confirms the accuracy of our iBEM method through cross-validation. According to the specific heat change of the PCM, when temperature is higher than the upper bound of the phase change window, the PCM particle behaves as an inhomogeneity in the domain. During this stage, although the temperature curve is sinusoidal, a slight phase delay exists inside the concrete compared to top surface temperature due to thermal diffusion. As the ambient temperature decreases, the PCM particle starts to solidify and the specific heat increases rapidly, performing as a heat sink, which prevents the decrease of the temperature. When the latent heat is released, the temperature curve becomes sinusoidal again until the next phase change process. The FEM and iBEM provide the similar prediction of the temperature change, which agree well with the experiments of the temperature at the center of the PCM particle in Fig. 4a. However, the slight difference is observed at 1cm right or lower to the PCM particle. It can be caused by the assumption of the uniform properties and temperature gradient field on the PCM particle, in which the moving phase change boundary is not considered. Because only one small PCM particle is used in the experiment, the influence of the phase change process to the entire temperature field is limited. However, the slope change of the temperature curve during the phase change process can be observed in Fig. 4a. To consider par-





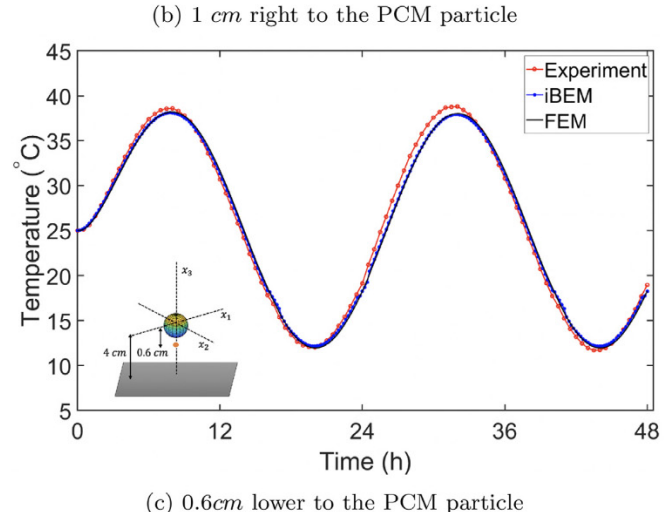


Fig. 4. Comparison of the temperature change with time at 3 locations shown in Fig. 2 by the experiment v.s. the iBEM and FEM predictions.

ticle interactions in actual composites, multiple PCM particles are considered in the following.

6.2. Verification of the temperature field with particle interactions

In the previous section, the iBEM has been compared to both the experimental and the FEM prediction of the temperatures at three locations of single PCM particle. To further illustrate the validity of the aforementioned algorithm under multiple particle interactions, 7 1cm - diameter PCM particles were placed around the

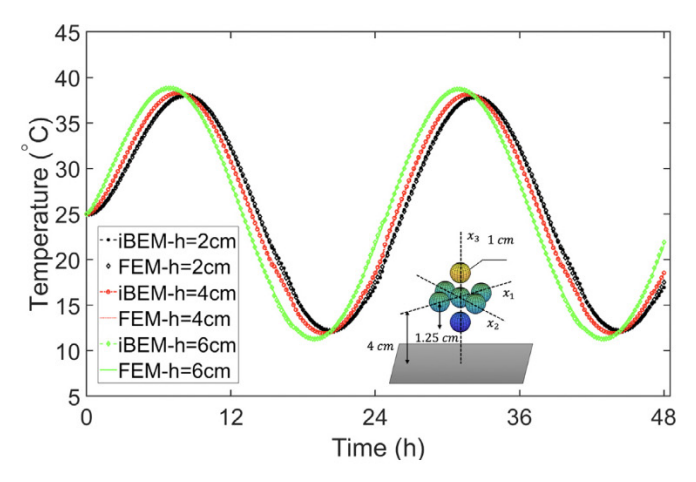


Fig. 5. Comparison of the variation of temperatures with time at 3 heights (2,4,6cm) under particle interactions.

center of the box, shown in Fig. 5. And the variations of temperature fields along the height direction have been compared with the FEM results under the same boundary conditions as Section 6.1. Notice that the temperature fields at near height are showing close results, therefore the curves only exhibit fields at 2,4,6 cm from the bottom surface. However, to keep consistent with the heat capacity method, the phase change process in both methods are simulated by a averaged piece-wise specific heat function of 4-degree phase change temperature window [16, 20] °C. The horizontal and vertical distance between neighbor particles are one-quarter of the radius as 0.25cm. At the three locations, temperature curves agree well with each other. Before the phase change process, the temperature curves were similar to the sinusoidal function, and temperature fields at different height exhibit obvious phase lag due to the thermal diffusion. During the phase change process, the temperature at 4cm height which has more interactions (center of the 7 particles), exhibits a slope change starting at 20 °C due to sudden increase of the heat capacity and ending at 16 °C, and the pattern repeat in next period. The maximum temperature of the second period decreases by 0.1 °C due to the phase change effect. Notice that iBEM involves solving a linear equation system with a full matrix, while FEM uses a sparse matrix, because the degree of freedom of iBEM is much smaller, and no mesh is needed, iBEM is particularly convenient for virtual experiments of PCM composites with random particle distributions.

7. Energy prediction of a PCM-concrete wall

The implementation of the iBEM algorithm is verified in the previous section with the FEM and experimental results under the sinusoidal temperature, insulated boundary conditions. However, in industrial applications, wall panels are subjected to air convection at both indoor and outdoor surfaces, as well as heat conduction and irradiation with the environment. The key design factor of an energy efficient building is the energy consumed to remain a desirable indoor temperature, i.e. 20 °C in this paper. In order to simulate a daily energy consumption, the boundary conditions are changed as follows, (i) The outdoor sinusoidal ambient temperature, $u(t) = 20 + 10Sin(\frac{\pi t}{12} - \frac{2\pi}{3})$. (ii)Absorbed sunlight (for 9 h) heat flux, $q(t) = 52Sin(\frac{\pi t}{12}), t \in [8, 17],$ (iii) Constant indoor temperature 20 °C, (iv) All side surfaces insulated for a 1-d heat transfer. The heat transfer coefficients are $h_i = 8W/m^2$ and $h_0 = 20W/m^2$ for indoor and outdoor concrete surfaces, respectively. The h_i is consistent with experimental measurement of mixed and natural convection [8,41] and h_0 [42,43] was obtained through the numerical simulation of walls under the outdoor weather condition.

7.1. Virtual experiment setup with boundary condition and energy measurement

The convection type boundary condition is defined as, the heat transfer rate, $\dot{Q} = hA\Delta u$, where $\Delta u = u_s - u_\infty$ is the temperature difference between indoor surface and near-surface air temperature. As the temperature difference in each time step is implicit, an iteration algorithm is needed. As a BEM-based method, the algorithm to solve the matrix is to separate unknown parameters. Based on the BEM algorithm, one modification can be made to solve the convection problems (at the observing time t_F) following Eq. (15).

$$\begin{split} [H_{nor}, H_{con}, J, M]_F[u_{nor}, u_{con}, \epsilon^*, Q^*]_F - [G_{nor}, G_{con}]_F[q_{nor}, q_{con}]_F \\ + \sum_{f=1}^{F-1} ([H, J, M]_f[u, \epsilon^*, Q^*]_f - [G]_f[q]_f) = [0] \end{split}$$

$$[H_{nor}, H_{con} + \frac{h}{k}G_{con}, J, M]_{F}[u_{nor}, u_{con}, \epsilon^{*}, Q^{*}]_{F} - [G_{nor}, 0]_{F}[q_{nor}, 0]_{F}$$

$$+ \sum_{f=1}^{F-1} ([H, J, M]_{f}[u, \epsilon^{*}, Q^{*}]_{f} - [G]_{f}[q]_{f}) = [0] - \frac{h}{k}[G_{con}]_{F}[u_{\infty}]_{F}$$

where, the subscript *nor* stands for boundary conditions with prescribed temperature or the temperature gradient, and the subscript *con* represents the convective boundary condition; u_{∞} is the convection film temperature. Substituting the definition equation of air equation above into the q_{con} , the BEM coefficient matrix at F time step changes accordingly by relating the convection surface node temperature with $H_F + G_{con}^F \frac{h}{k}$ and all other parameters in the matrix remain the same.

Three case studies are launched to investigate the influence of the volume fraction and location of the PCM particles on the heat transfer and energy consumption through a builiding wall. In the first study, energy consumption and temperature at various heights of the different volume fraction (Φ_p) of 0%, 5%, 10%, 15% and 20% are compared. Considering the real application, the non-overlapping PCM particles are randomly generated in terms of both positions and diameters (ranging between [0.5, 0.75]cm). Thus, in each case of different volume fractions, 0,15,28,41 and 57 particles are generated in the domain with a narrower dimension

 $L \times W \times H = 2 \times 2 \times 8cm$, where the 1-d heat transfer happens at z - axis with a height of 8cm. The material thermal properties of the PCM particles changes in the phase change temperature window of [18, 22] °C; otherwise they remain the same. The thermal properties of the concrete is temperature independent. In the second case study, the effect of phase change temperature window is investigated. Defined in Section 4, the phase change temperature window is $[u_s, u_e]$, and it could be further split as $[u_c - \Delta u, u_c + \Delta u]$, where $u_c = \frac{u_s + u_e}{2}$ and $\Delta u = \frac{u_e - u_s}{2}$ are introduced as the melting temperature (midpoint of the phase change window) and range of phase change temperature around the u_c . In order to study the influence of the phase change temperature range Δu , the authors fix $u_c = 20$ °C and change $\Delta u = 0.5, 1, 2$ when the volume fraction of PCM $\Phi_p = 0.10$ under the same boundary conditions of the first case study. The temperature at the center and indoor heat flux are compared in the 5 cases. As for the third case study, 23 particles are randomly generated in the box domain $(L \times W \times H = 2 \times 2 \times 2)$ cm)shown in Fig. 10, with diameter falls in the range [0.4, 0.6]cm, then through adjusting the heights of the 23 particles at 5 different levels (1, 2, 3, 4, 5cm), the indoor heat flux curves are compared with the one with random distribution of the same volume fraction $\Phi_p = 7.5\%$.

7.2. The effect of the PCM volume fraction

Since the PCM particles are randomly placed in the sample domain, the indoor heat flux is measured through averaging the boundary responses (temperature gradient) multiplied with thermal conductivity k. Shown in Fig. 6, the virtual experiment monitors the 24-hour heat flux change, between the noon t = 12pmand t = 12pm(+1). When $\Phi_p = 0$, the indoor heat flux curves is the a sinusoidal function of time with a phase delay due to the thermal diffusion. With the increase of the Φ_p , an obvious trend is observed that the peak heat flux in both positive/negative parts reduces gradually. The maximum difference of the peak flux occurs in the $\Phi_p = 20\%$ curve, with heat flux reduction up to $25.01W/m^2$ compared to the plain wall. The phase change temperature window is set as [18, 22] °C. It is noted that phase lags exist in all PCMembedded cases except the $\Phi_p=20\%$ one. One explanation is that when the temperature at higher location are in the phase change process, larger volume of PCM particles absorbs more heat, which leads to the particles at lower height stays in the phase change

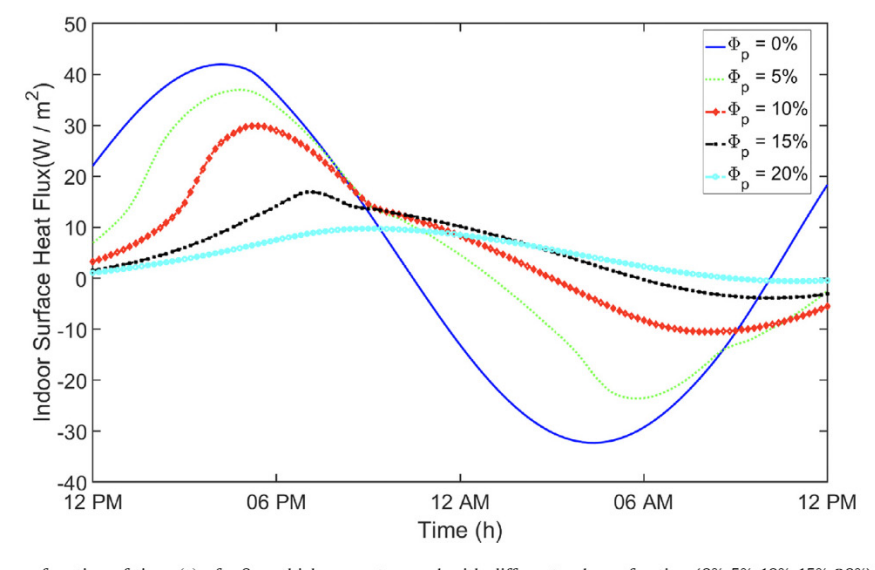


Fig. 6. Indoor surface heat flux as a function of time (t) of a 8cm-thick concrete panel with different volume fraction (0%, 5%, 10%, 15%, 20%) of PCM particles, here the latent heat is 160kJ/kg, $u_c = 20 \,^{\circ}\text{C}$ and $\Delta u = 2 \,^{\circ}\text{C}$.

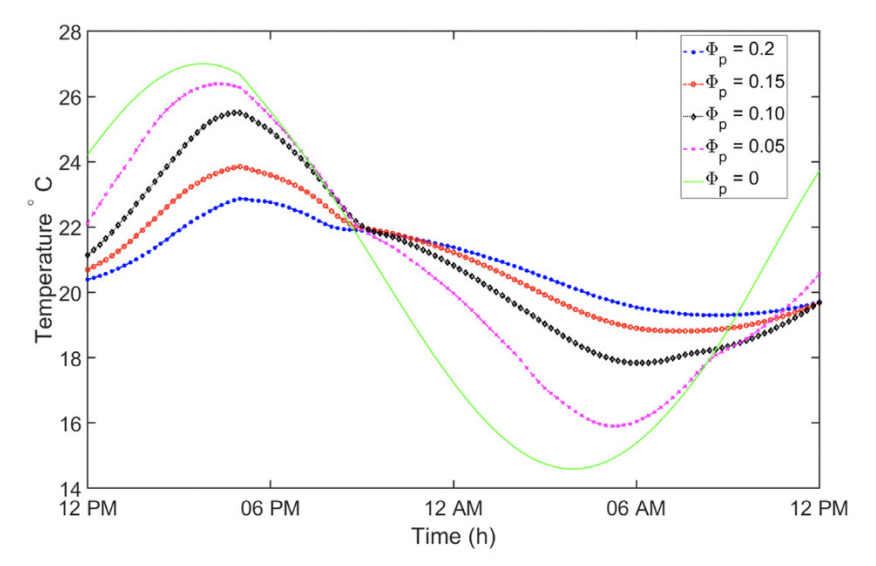


Fig. 7. Temperature at the center of the sample as a function of time (t) of a 8cm-thick concrete panel with different volume fraction (0%, 5%, 10%, 15%, 20%) of PCM particles, here the latent heat is fixed as 160kJ/kg, $u_c = 20 \,^{\circ}\text{C}$ and $\Delta u = 2 \,^{\circ}\text{C}$.

Table 2Energy consumption by the integral of averaged indoor heat flux in 24 h with different volume fraction of randomly distributed PCM particles.

$\Phi_p = 0\%$	5%	10%	15%	20%
0.564kW · h	$0.415kW \cdot h$	0.284kW h	0.171 <i>kW</i> · <i>h</i>	0.116 <i>kW</i> · <i>h</i>

process in the entire period. Therefore, the heat flux curve with $\Phi_p = 20\%$ also performs as a sinusoidal function without phase lags due to absence of the phase change. Other heat flux curves, experiencing the phase change process, show the phase delay of the peak heat flux, i.e., 0.6, 1, 2.8h for $\Phi_p = 5\%$, 10%, 15%, respectively. Fig. 7 shows the variation of temperature at the center of the sample domain, the same trend is observed that higher volume fraction of PCM particles reduces the peak temperature and shift the phase later. However, the phase delay is relatively smaller than the heat flux one since the temperature field is compared at h = 4cm. In the second half of the period, the phase change lags of $\Phi_p = 15\%, 20\%$ are not observed due to the larger mass PCM particles serving as heat source, which reduces the peak negative temperature amplitude. The overall energy input needed for the room to maintain 20°C can be calculated by integrating the absolute indoor flux with time. As we can see in the Table 2, by adding PCM particles in a building wall, we can reduce building energy consumption by 79% when 20% PCM is used.

7.3. The effect of phase change temperature window

In this section, the scale of the phase change window is modified to investigate its influence on the indoor surface heat flux and temperature field at the center of the PCM-concrete wall. Based on Eq. (7), changing Δu leads to different values of the specific heat to match the same latent heat during the phase change process. A higher material mismatch, shown in Eq. (9), causes a larger eigen heat source term Q_f^{l*} in the phase change process, resulting in sudden larger slope change of both temperature and heat flux field. Shown in Fig. 8, the heat flux curve with smaller phase change temperature window tends to have a flattened slope at the beginning, and the reason is that during the first 2-3h, most PCM particles are in the mushy status, which absorbs the heat causing a smaller change of the heat flux field. In addition, a smaller Δu enlarges the specific heat since the total latent heat remains

Table 3Energy consumption by the integral of averaged indoor heat flux in 24 h with phase change temperature window of randomly distributed PCM particles.

$\Delta u \Phi_p = 0\%$	0.5°C	1°C	1.5°C	2°C
0.564kW · h	0.210kW · h	0.227kW h	0.248kW · h	0.284kW · h

the same. Then, the heat flux field of smaller phase change window ends the phase change process sooner due to a comparatively small phase change temperature window. After the phase change process, the heat flux increases more rapidly than others that have larger phase change window, and the peak heat fluxes are equivalent in all curves with $\Phi_p = 10\%$. As mentioned in Section 7.2, the phase change process exists when the temperature decreases around 10PM, and the opposite trend is observed here that the heat flux curve with smaller Δu begins the phase change process later. However, it could be resulted from the effect of the fixed u_c in the sense that a smaller Δu requires the temperature of the PCM particles to drop below $u_c + \Delta u$. The temperature field, seen in Fig. 9, exhibits a similar same trend as the heat flux field. Initially, the four curves almost overlap, which is due to the effect of the uniform initial condition. By integrating the absolute indoor flux with time, the overall energy consumption required to maintain the thermal comfort at 20 °C could be obtained. As shown in Table 3, with smaller Δu , more energy could be saved. For example, given the same latent heat, a PCM with a phase change window $\Delta u = 0.5$ °C would reduce 13% more building enerngy consumption than one with $\Delta u = 2 \,^{\circ}$ C.

It is interesting to note that this finding differs from previous claims that phase change temperature window has insignificant effects on the energy flux reduction and phase delay of PCM-concrete composites [8]. It is speculated from our study that such statement should be conditioned on the assumptions that (i) the melting temperature of PCM u_c is lower enough than the sinusoidal peak temperature, and (ii) the daily temperature fluctuation range should fully cover the phase change window of the PCM. When u_c is close to the peak temperatures, we may take advantage of our current finding and design PCMs with optimized phase change temperature window to maximize energy savings achieve desirable delay in peak energy flux, so that we could achieve maximized cost savings while stabilizing the power grid.

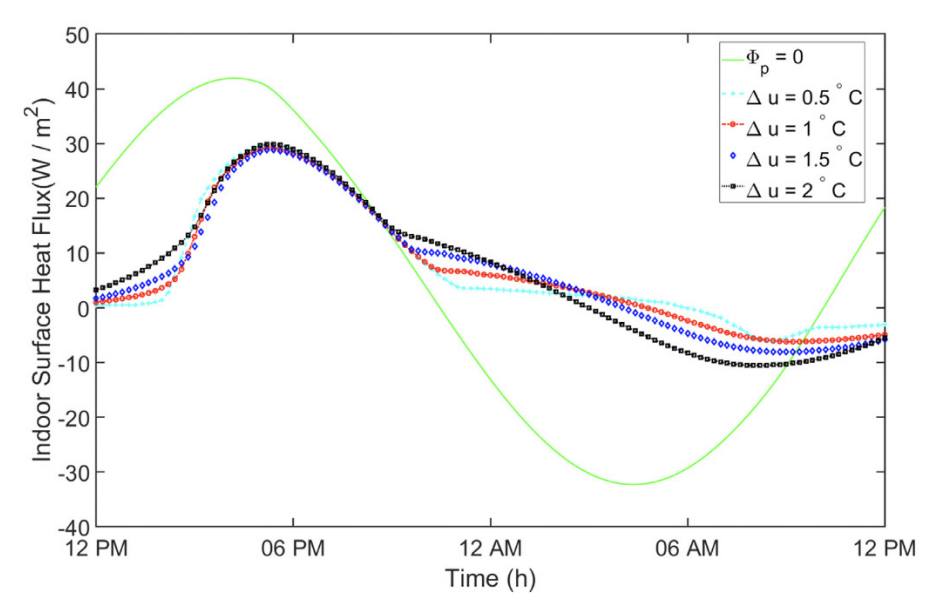


Fig. 8. Indoor surface heat flux as a function of time (t) of a 8cm-thick concrete panel with various phase change temperature window length $(\Delta u = 0.5, 1, 1.5, 2\,^{\circ}\text{C})$, here the latent heat is 160kJ/kg, $u_c = 20\,^{\circ}\text{C}$.

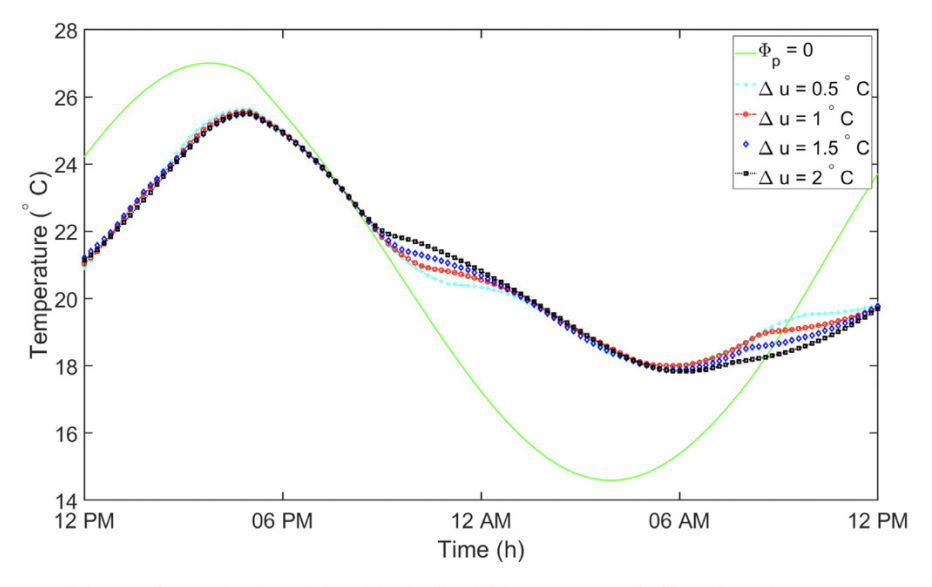


Fig. 9. Temperature at the center of the sample as a function of time (t) of a 8cm-thick concrete panel with various phase change temperature window length ($\Delta u = 0.5, 1, 1.5, 2$ °C), here the latent heat is 160kJ/kg, $u_c = 20$ °C.

7.4. The effect of particles distribution within a wall

In this section, 23 PCM particles are randomly generated in a small cube 2cm. These particles took up 30% of the cube, which itself was part of a $2 \times 2 \times 8cm$ simulation box to mimick a 8cmthick wall. Thus the PCM volume fraction in the entire wall was $\Phi_p = 7.5\%$. Shown in Fig. 10, the distance between the small cube center to the indoor surface is h, through changing the height of the cube, the indoor heat flux are monitored. To better illustrate the effect of particle gathering, location, the author create another case of random distributed $\Phi_p = 7.5\%$ PCM particles. It is observed that when the PCM particles are closer to the indoor surface, not only the peak heat flux field decreases but also the effect shift the phase later. The similar trend is shown in the case of increasing the volume fraction of PCM particles. However, the volume fraction is only 7.5%, such amount of PCM particles fails to reproduce the same phenomenon as seen in Fig. 6, as the overall latent heat are not sufficient to absorb the heat which keeps the indoor neighbor temperature inside the phase change temperature window. The energy consumption is provided as Table 4. Because the phase change temperature is close to the desirable room temperature, When the PCM particles are concentrated to the indoor surface, it produces the highest energy saving at 0.564-0.183=0.381kW.h; whereas h=5cm at 0.564-0.328=0.236kW.h. A 50% increase of energy saving to move the PCM cube from the outside surface to inside can be obtained. Notice that the randomly distributed PCM configuration produces the lowest energy saving although the uniform particle distribution provides benefits in mechanical and structural performance and manufacturing process. This is common that laminate materials/structures perform favorably from the homogeneous alternatives for heat insulation.

Given a specific daily temperature change pattern, the energy saving and phase delay can be significantly changed by PCM's phase change temperature window, volume fraction, and distribution. Optimization of the PCM-concrete design might lead to large saving for energy efficient buildings. The iBEM algorithm provides

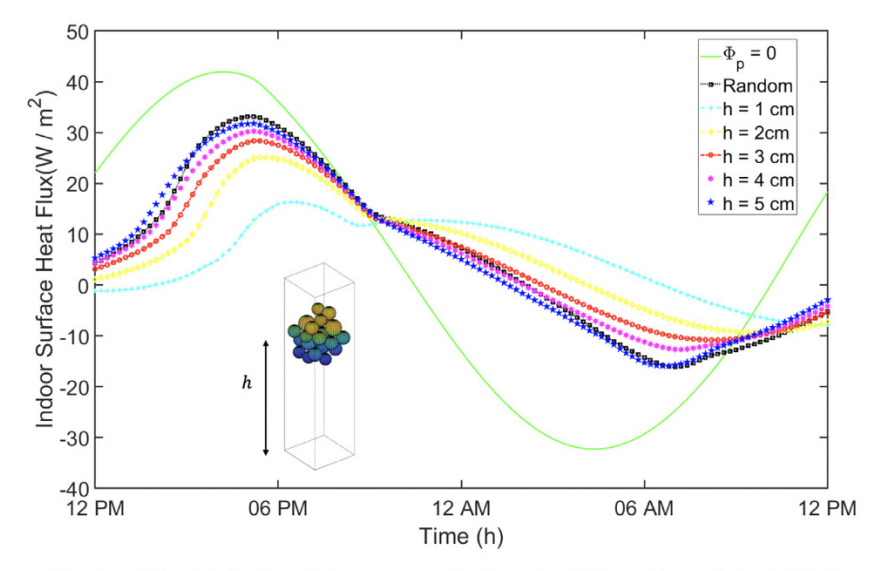


Fig. 10. Indoor surface heat flux as a function of time (t) of a 8cm-thick concrete panel with various PCM particles gathering height, here specific heat 160kJ/kg, $u_c = 20\,^{\circ}$ C and $\Delta u = 2\,^{\circ}$ C.

Table 4Energy consumption by the integral of averaged indoor heat flux in 24 h with various PCM particles gathering height.

Height (cm) 1	2	3	4	5	random
$0.183kW \cdot h$	0.243kW · h	0.276kW · h	0.301 <i>kW</i> · <i>h</i>	0.328kW · h	0.339kW · h

a powerful tool for virtual experiments of different material designs.

8. Conclusions

The algorithm of phase change process has been implemented in the iBEM to investigate the transient heat transfer problem of PCM particle embedded concrete for energy efficient building envelope applications. The present method was verified with the experiments and FEM simulations. For a prescribed domain with known PCM particle, the heat field can be solved with iBEM and the heat source algorithm. Rather than meshing the inhomogeneity to multiple of grids, the inhomogeneities are treated as same material of the matrix with an eigen-temperature gradient and fictitious heat source. Hence, the same BEM model can be used in iBEM for virtual experiments of material sample with multiple PCM particles. The iBEM is verified by FEM and validated by the experiments. The virtual experiments show that iBEM can be a powerful tool for the design and optimization of PCM-concrete composites, which can lead to 50% energy saving with microstructure optimization for the specific example. The effect of volume fraction, phase change temperature window, and particle concentration zone on the energy consumption and phase delay are illustrated.

Declaration of Competing Interest

The authors declare that they have no known competing financial interests or personal relationships that could have appeared to influence the work reported in this paper.

CRediT authorship contribution statement

Chunlin Wu: Writing - original draft, Methodology, Data curation. **Zhenhua Wei:** Methodology, Writing - review & editing, Validation. **Huiming Yin:** Funding acquisition, Conceptualization, Project administration, Writing - review & editing.

Acknowledgements

This work is sponsored by the National Science Foundation IIP 1738802 and CMMI 1762891, whose support is gratefully acknowledged.

Appendix A. Explicit time-integral form of G, T and discussion of singularity

The explicit time integrals of the Green's function and its derivative are provided as follows [27],

$$\overline{G}(\mathbf{r}, t_{\Omega}, \Delta t) = \int_{t_f - 1}^{t_f} G(\mathbf{r}, \tau) dt$$

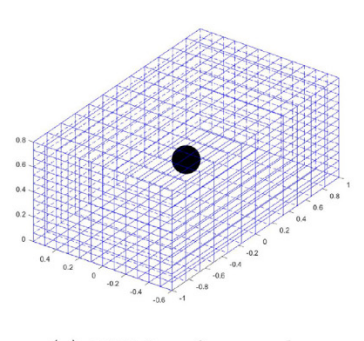
$$= \frac{1}{4\alpha r \pi^{\frac{3}{2}}} \left[\Gamma\left(0.5, \frac{r^2}{4\alpha (t_{\Omega} + \Delta t)}\right) - \Gamma\left(0.5, \frac{r^2}{4\alpha t_{\Omega}}\right) \right] \tag{A.1}$$

$$\overline{T}(\mathbf{r}, t_{\Omega}, \Delta t) = \int_{t_{f}-1}^{t_{f}} T(\mathbf{r}, \tau) dt$$

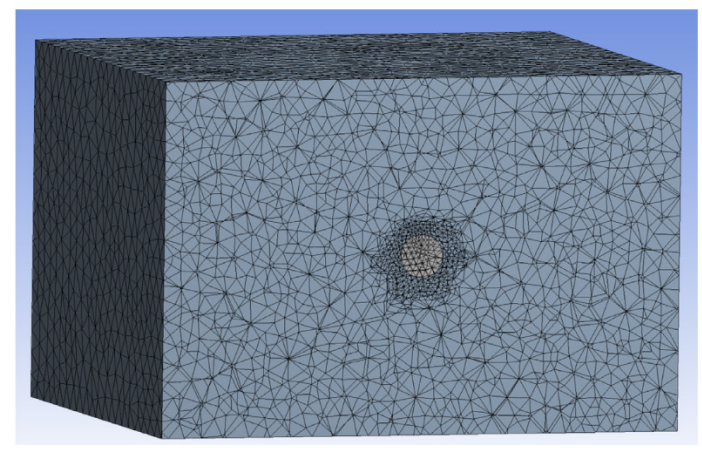
$$= \frac{\mathbf{r} \cdot \mathbf{n}}{2\alpha r^{3} \pi^{\frac{3}{2}}} \left[\Gamma\left(1.5, \frac{r^{2}}{4\alpha (t_{\Omega} + \Delta t)}\right) - \Gamma\left(1.5, \frac{r^{2}}{4\alpha t_{\Omega}}\right) \right] \tag{A.2}$$

where Γ is the upper incomplete gamma function.

Because the Green's function is singular at the source points, the integrals over spatial domain should be carefully conducted. The singularities can be divided into two kinds, weakly singular and strongly singular. As for weakly singular, the integral of the kernel function poses no problem [35], and the approach will not be discussed here. However, the strongly singular generates problems in numerical implementation, and Beer proposed to use method of rigid body motion, which creates one uniform temperature field (similar to displacement in elastic problem) with zero gradient. Thus, the diagonal elements in \overline{H} , C can be expressed by negative summation of all other elements in the same row. The merit of the method is not only save computation resources for strongly singular but also avoid errors in matrix C of direct



(a) iBEM surface mesh



(b) FEM volume mesh

Fig. B.11. Schematic illustration of surface/volume mesh for the iBEM and FEM for one PCM particle case.

BEM method. The method of rigid motion works well with steadystate problems, but modifications are required for its application on transient problems. Dargush and Banerjee proposed the method to seperate the kernel integral into two parts, where one is timedependent and the other is time-independent [44]. Similarly, the kernel function for boundary nodes' temperature can be separated as.

$$\int_{\partial D} \overline{T}(\mathbf{r}, t_{\Omega}, \Delta t) ds = \int_{\partial D} \frac{\mathbf{r} \cdot \mathbf{n}}{2\alpha r^{3} \pi^{\frac{3}{2}}} \left[-\gamma \left(1.5, \frac{r^{2}}{4\alpha (t_{\Omega} + \Delta t)} \right) + \gamma \left(1.5, \frac{r^{2}}{4\alpha t_{\Omega}} \right) \right] ds$$
(A.3)

where $\Gamma(s), \gamma(s)$ are complete gamma function and lower incomplete gamma function and $\Gamma(s,t)=\Gamma(s)-\gamma(s,t)$ is applied. In most cases that $t_\Omega=t_F-t_f\neq 0$ (not the first coefficient matrix), the Eq. (A.3) does not have singular as the entire asymptotic series is $O(r^3)$. Whens the time step coincide, $\gamma(1.5,\frac{r^2}{4\alpha t_\Omega})=\gamma(1.5,\infty)\approx \Gamma(1.5)$, which is a constant in the integral equation. Therefore, there exist strong singularities and it can be solved by seperating constant and lower incomplete gamma function series as, (F-f=0.5)

$$\int_{\partial D} \overline{T}(\mathbf{r}, 0, \Delta t) = \int_{\partial D} \frac{\mathbf{r} \cdot \mathbf{n}}{4\alpha r^3 \pi} ds - \int_{\partial D} \gamma (1.5, \frac{r^2}{4\alpha (t_{\Omega} + \Delta t)}) ds$$
(A.4)

where the first term in Eq. (A.4) is the similar term derived in steady-state heat conduction problems. Similarly, the \overline{H} matrix can be divided into 'steady-state' and 'transient' part, and the method of rigid body motion can only be applied to the 'steady-state' part. As a consequence of applying method of rigid body motion directly on \overline{H} , the solved heat field will be steady-state.

Appendix B. Comparison of the mesh for the experiment verification

In Section 6.1, a verification was performed with the iBEM, FEM and experiment. Shown in Fig. B.11, the iBEM only requires a surface mesh and the number of element seeds on each edge is 12, thus 144 elements are generated for each surface with totally 866 nodes. The particles in the domain, are treated as just 4 unknowns of the eigen field, therefore no internal mesh is needed. The same surface mesh for iBEM could be used for various cases unless the external geometry changes. However, the FEM requires the internal

volume mesh. With just one particle, the volume mesh includes 49342 elements. Considering more particles with size gradation, it is quite challenging since the difference between neighbor element sizes is strictly limited for accuracy purposes.

References

- U.E.I. Administration, Residential Energy Consumption Survey, Technical Report, 2015.
- [2] M.A. Sharif, A. Al-Abidi, S. Mat, K. Sopian, M. Ruslan, M. Sulaiman, M. Rosli, Review of the application of phase change material for heating and domestic hot water systems, Renew. Sustain. Energy Rev. 42 (2015) 557–568, doi:10.1016/j.rser.2014.09.034.
- [3] J. Kośny, PCM-Enhanced Building Components, Springer International Publishing, 2015, doi:10.1007/978-3-319-14286-9.
- [4] C.A. Ikutegbe, M.M. Farid, Application of phase change material foam composites in the built environment: a critical review, Renew. Sustain. Energy Rev. 131 (2020) 110008, doi:10.1016/j.rser.2020.110008.
- [5] Y. Cui, J. Xie, J. Liu, J. Wang, S. Chen, A review on phase change material application in building, Adv. Mech. Eng. 9 (6) (2017), doi:10.1177/1687814017700828
- [6] C. Voelker, O. Kornadt, M. Ostry, Temperature reduction due to the application of phase change materials, Energy Build. 40 (5) (2008) 937–944, doi:10.1016/j. enbuild.2007.07.008.
- [7] S.-G. Jeong, J. Jeon, J. Cha, J. Kim, S. Kim, Preparation and evaluation of thermal enhanced silica fume by incorporating organic PCM, for application to concrete, Energy Build. 62 (2013) 190–195, doi:10.1016/j.enbuild.2013.02.053.
- [8] A.M. Thiele, G. Sant, L. Pilon, Diurnal thermal analysis of microencapsulated PCM-concrete composite walls, Energy Convers. Manage. 93 (2015) 215–227, doi:10.1016/j.enconman.2014.12.078.
- [9] M.M. Farid, A.M. Khudhair, S.A.K. Razack, S. Al-Hallaj, A review on phase change energy storage: materials and applications, Energy Convers. Manage. 45 (9-10) (2004) 1597–1615, doi:10.1016/j.enconman.2003.09.015.
- [10] S.N. AL-Saadi, Z.J. Zhai, Modeling phase change materials embedded in building enclosure: a review, Renew. Sustain. Energy Rev. 21 (2013) 659–673, doi:10. 1016/j.rser.2013.01.024.
- [11] Y. Cui, J. Xie, J. Liu, S. Pan, Review of phase change materials integrated in building walls for energy saving, Procedia Eng. 121 (2015) 763–770, doi:10. 1016/j.proeng.2015.09.027.
- [12] H. Hu, S.A. Argyropoulos, Mathematical modelling of solidification and melting: a review, Modell. Simul. Mater. Sci.Eng. 4 (4) (1996) 371–396, doi:10.1088/0965-0393/4/4/004.
- [13] V.R. Voller, C.R. Swaminathan, B.G. Thomas, Fixed grid techniques for phase change problems: a review, Int. J. Numer. MethodsEng. 30 (4) (1990) 875–898, doi:10.1002/nme.1620300419.
- [14] S.R. Idelsohn, M.A. Storti, L.A. Crivelli, Numerical methods in phase-change problems, Arch. Comput. Methods Eng. 1 (1) (1994) 49–74, doi:10.1007/ bf02736180.
- [15] V. Alexiades, A.D. Solomon, Mathematical Modeling of Melting and Freezing Processes, Routledge, 2018, doi:10.1201/9780203749449.
- [16] V. Voller, J. Swenson, W. Kim, C. Paola, An enthalpy method for moving boundary problems on the Earth's surface, Int. J. Numer. Methods HeatFluid Flow 16 (5) (2006) 641–654, doi:10.1108/09615530610669157.
- [17] V.R. Voller, Fast implicit finite-difference method for the analysis of phase change problems, Numer. Heat Transf. Part B 17 (2) (1990) 155–169, doi:10. 1080/10407799008961737.

- [18] C. Swaminathan, V. Voller, On the enthalpy method, Int. J. Numer. Methods Heat Fluid Flow 3 (3) (1993) 233–244, doi:10.1108/eb017528.
- [19] D. Knoll, D. Keyes, Jacobian-free Newton-Krylov methods: a survey of approaches and applications, J. Comput. Phys. 193 (2) (2004) 357–397, doi:10.1016/j.jcp.2003.08.010.
- [20] J.S. Hsiao, An efficient algorithm for finite-difference analyses of heat transfer with melting and solidification, Numer. Heat Transf. 8 (6) (1985) 653–666, doi:10.1080/01495728508961877.
- [21] A. Faghri, Y. Zhang, 6 melting and solidification, in: A. Faghri, Y. Zhang (Eds.), Transport Phenomena in Multiphase Systems, Academic Press, Boston, 2006, pp. 421–530, doi:10.1016/B978-0-12-370610-2.50011-8.
- [22] C. Swaminathan, V. Voller, Towards a general numerical scheme for solidification systems, Int. J. Heat Mass Transf. 40 (12) (1997) 2859–2868, doi:10.1016/s0017-9310(96)00329-8.
- [23] M. Costa, D. Buddhi, A. Oliva, Numerical simulation of a latent heat thermal energy storage system with enhanced heat conduction, Energy Convers. Manage. 39 (3-4) (1998) 319-330. doi:10.1016/s0196-8904(96)00193-8.
- [24] G. Beckett, J. Mackenzie, M. Robertson, A moving mesh finite element method for the solution of two-dimensional stefan problems, J. Comput. Phys. 168 (2) (2001) 500–518, doi:10.1006/jcph.2001.6721.
- [25] R. Merle, J. Dolbow, Solving thermal and phase change problems with the eXtended finite element method, Computational Mechanics 28 (5) (2002) 339– 350. doi:10.1007/s00466-002-0298-v.
- [26] W. Yao, B. Yu, X. Gao, Q. Gao, A precise integration boundary element method for solving transient heat conduction problems, Int. J. Heat Mass Transf. 78 (2014) 883–891, doi:10.1016/j.ijheatmasstransfer.2014.07.029.
- [27] A. Gupta, J.M. Sullivan, H.E. Delgado, An efficient bem solution for threedimensional transient heat conduction, Int. J. Numer. Methods Heat Fluid Flow 5 (4) (1995) 327–340. doi:10.1108/eum0000000004069.
- [28] F.Y. Saptaningtyas, A.D. Setyarsi, Finite volume method with explicit scheme technique for solving heat equation, J. Phys. 1097 (2018) 012089, doi:10.1088/ 1742-6596/1097/1/012089.
- [29] J.D. Eshelby, The determination of the elastic field of an ellipsoidal inclusion, and related problems, Proc. R. Soc. London Ser.A 241 (1226) (1957) 376–396, doi:10.1098/rspa.1957.0133.
- [30] H. Hatta, M. Taya, Thermal conductivity of coated filler composites, J. Appl. Phys. 59 (6) (1986) 1851–1860, doi:10.1063/1.336412.
- [31] H. Hiroshi, T. Minoru, Equivalent inclusion method for steady state heat conduction in composites, Int. J. Eng. Sci. 24 (7) (1986) 1159–1172, doi:10.1016/0020-7225(86)90011-x.

- [32] G. Song, L. Wang, L. Deng, H. Yin, Mechanical characterization and inclusion based boundary element modeling of lightweight concrete containing foam particles, Mech. Mater. 91 (2015) 208–225, doi:10.1016/j.mechmat.2015.07.014.
- [33] G. Song, H.M. Yin, Stress concentration of one microvoid embedded in an adhesive layer under harmonic load, J. Eng. Mech. 144 (3) (2018) 04018002, doi:10.1061/(asce)em.1943-7889.0001416.
- [34] G. Song, Inclusion-based boundary element method (iBEM) for composite materials, Columbia University, 2017 Ph.D. thesis.
- [35] I.M.S. Gernot Beer, C. Duenser, The Boundary Element Method with Programming, Springer Vienna, 2008, doi:10.1007/978-3-211-71576-5.
- [36] H.M. Yin, G.H. Paulino, W.G. Buttlar, L.Z. Sun, Effective thermal conductivity of functionally graded particulate nanocomposites with interfacial thermal resistance, I. Appl. Mech. 75 (5) (2008). doi:10.1115/1.2936893.
- [37] H. Yin, G. Paulino, W. Buttlar, L. Sun, Heat flux field for one spherical inhomogeneity embedded in a functionally graded material matrix, Int. J. Heat Mass Transf. 51 (11–12) (2008) 3018–3024, doi:10.1016/j.ijheatmasstransfer.2007.09.
- [38] A.M. Thiele, Z. Wei, G. Falzone, B.A. Young, N. Neithalath, G. Sant, L. Pilon, Figure of merit for the thermal performance of cementitious composites containing phase change materials, Cem. Concr. Compos. 65 (2016) 214–226, doi:10.1016/j.cemconcomp.2015.10.023.
- [39] M. Tanaka, T. Matsumoto, Q.F. Yang, Time-stepping boundary element method applied to 2-D transient heat conduction problems, Appl. Math. Modell. 18 (10) (1994) 569–576, doi:10.1016/0307-904x(94)90142-2.
- [40] K. Kumarasamy, J. An, J. Yang, E.-H. Yang, Numerical techniques to model conduction dominant phase change systems: A CFD approach and validation with DSC curve, Energy Build. 118 (2016) 240–248, doi:10.1016/j.enbuild.2016.02.040
- [41] H. Awbi, A. Hatton, Mixed convection from heated room surfaces, Energy Build. 32 (2) (2000) 153–166, doi:10.1016/s0098-8472(99)00063-5.
- [42] E.M. Alawadhi, Thermal analysis of a building brick containing phase change material, Energy Build. 40 (3) (2008) 351–357, doi:10.1016/j.enbuild.2007.03.
- [43] L. Hembade, N. Neithalath, S.D. Rajan, Understanding the energy implications of phase-change materials in concrete walls through finite-element analysis, J. Energy Eng. 140 (1) (2014) 04013009, doi:10.1061/(asce)ey.1943-7897.0000146.
- [44] G. Dargush, P. Banerjee, Boundary element methods in three-dimensional thermoelasticity, Int. J. Solids Struct. 26 (2) (1990) 199–216, doi:10.1016/ 0020-7683(90)90052-w.